International Journal of Nanomedicine

Dovepress
open access to scientific and medical research

Open Access Full Text Article

ORIGINAL RESEARCH

Enhanced Photothermal-Photodynamic Therapy by Indocyanine Green and Curcumin-Loaded Layered MoS_2 Hollow Spheres via Inhibition of P-Glycoprotein

This article was published in the following Dove Press journal:
International Journal of Nanomedicine

Shuai Li[1,*]
Shuping Yang[2,*]
Chong Liu[1]
Jintong He[1]
Tian Li[1]
Changhui Fu[3]
Xianwei Meng[3]
Haibo Shao[1]

[1]Department of Interventional Radiology, The First Hospital of China Medical University, Shenyang 110001, Liaoning, People's Republic of China; [2]Department of Pain Medicine, The First Hospital of China Medical University, Shenyang 110001, Liaoning, People's Republic of China; [3]Laboratory of Controllable Preparation and Application of Nanomaterials, Chinese Academy of Sciences Key Laboratory of Cryogenics, Technical Institute of Physics and Chemistry, Chinese Academy of Sciences, Beijing 100190, People's Republic of China

*These authors contributed equally to this work

Correspondence: Haibo Shao
Department of Interventional Radiology, The First Hospital of China Medical University, Shenyang 110001, Liaoning, People's Republic of China
Email haiboshao@aliyun.com

Xianwei Meng
Laboratory of Controllable Preparation and Application of Nanomaterials, Chinese Academy of Sciences Key Laboratory of Cryogenics, Technical Institute of Physics and Chemistry, Chinese Academy of Sciences, Beijing 100190, People's Republic of China
Email mengxw@mail.ipc.ac.cn

Purpose: P-glycoprotein (P-gp), which is highly expressed in liver cancer cells, is one of the obstacles for the treatment of cancer. In this study, we have prepared and characterized a kind of novel ICG&Cur@MoS_2 (ICG and Cur represent indocyanine green and curcumin, respectively) nanoplatform, which can achieve photothermal-photodynamic therapy and inhibit the P-gp effectively and safely.

Methods: In this work, plenty of studies including drug release, acute toxicity, Western blot, real-time PCR, cell viability, therapeutic experiment in vivo, immunofluorescence and so on were conducted to test the antitumor potential of ICG&Cur@MoS_2 and the inhibitory effect of curcumin on P-gp.

Results: The ICG&Cur@MoS_2 NPs exhibit an excellent photothermal effect and relatively low toxicity. Cell viability in the ICG&Cur@MoS_2 + NIR group was significantly lower than that in ICG@MoS_2 + NIR group (75.3% vs 81.2%, 59.0% vs 64.4%, 20.3% vs 27.5%, and 15.4% vs 22.3%) at the concentration of ICG at 0.5, 5, 25, 50 μg/mL ($P<0.05$ at each concentration). Western blot, Q-PCR, and immunofluorescence assay indicate ICG&Cur@MoS_2 NPs can inhibit the P-gp effectively and safely. In vivo, the tumors in the ICG@MoS_2 + NIR group are significantly smaller than those in the MoS_2 + NIR group (95.0 vs 420.9 mm^3, $p<0.05$).

Conclusion: In conclusion, we have successfully synthesized ICG&Cur@MoS_2 nanoparticles which can not only achieve PTT-PDT but also inhibit P-gp effectively. Our findings indicate that the PTT-PDT exhibits great potential in the treatment of hepatocellular carcinoma. Meanwhile, ICG&Cur@MoS_2 can effectively inhibit the expression of P-gp, which will enhance the PDT effect.

Keywords: P-glycoprotein, hepatocellular carcinoma, indocyanine green, curcumin, MoS_2, photothermal-photodynamic therapy

Introduction

Phototherapy for hepatocellular carcinoma has attracted widespread attention because of its easy implementation without damage to normal organs.[1,2] Of all the phototherapeutic approaches, photothermal therapy (PTT) and photodynamic therapy (PDT) were in the spotlight.[3,4] The abundant blood supply of liver cancer will adversely affect thermal ablation. However, photodynamic therapy may benefit from this kind of oxygen-enriched microenvironment. Plenty of studies have tried to combine the above two ways to achieve better therapeutic effects.[5,6] However, most of the researches either

need multiple light sources or exhibit weak photodynamic effects resulted from photosensitizers efflux from the cancer cells mediated by membrane proteins such as p-glycoprotein (P-gp).[7,8] P-gp, which is encoded by the MDR1 gene,[9] is an ATP-dependent efflux pump and it is expressed in a wide variety of cancer cells. It can pump antitumor drugs out of cancer cells, which can induce multidrug resistance (MDR) finally. In order to overcome the above defects, we developed a PTT-PDT system involving ICG&Cur@MoS_2 nanoparticles (ICG and Cur represent indocyanine green and curcumin, respectively). In this work, layered MoS_2 hollow spheres (LMHSs) that have been studied in depth in our previous research were employed as photosensitizers carriers.[10,11] The LMHSs are developed with both layered and hollow structures, making it suitable for loading anticancer agents (Scheme 1). ICG and the LMHSs can be excited by an 808 nm near infrared (NIR) laser to simultaneously achieve PDT and PTT. Different from UV or visible light, NIR laser can penetrate more deeply into tissue while causing less damage to normal tissues, making it suitable for in vivo PTT and PDT. In view of the efficacy of PDT may be weakened by ICG's efflux from cancer cells mediated by P-gp, curcumin was hence loaded into the LMHSs to enhance the anti-cancer effect by inhibiting the activity of intracellular P-gp. P-gp inhibitors usually have a variety of adverse reactions. For instance, rifampin has severe hepatotoxicity in patients with liver dysfunction in addition to anorexia and nausea.[12] However, curcumin has less side effects compared with other P-gp inhibitors.[13,14] Therefore, it is used in the LMHSs to inhibit P-gp. In this work, plenty of studies including drug release, acute toxicity, cell viability, Western blot, real-time PCR, immunofluorescence, etc. were conducted to verify the anti-tumor effect of ICG&Cur@MoS_2. In summary, the ICG&Cur@MoS_2 may be a promising and powerful tool to treat liver cancer.

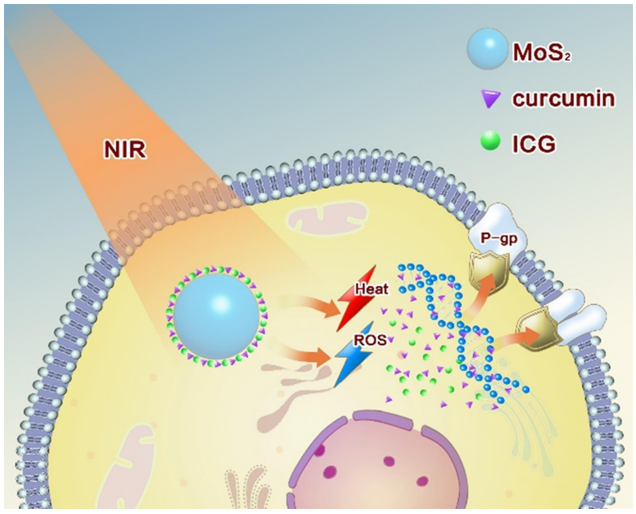

Scheme 1 ICG&Cur@MoS_2 nanoparticles were successfully synthesized. It realizes PTT-PDT and effectively inhibit P-gp. Cur is much safer than traditional P-gp inhibitors. The unique structure of LMHSs provides more space for anti-tumor agents. The PTT-PDT exhibits great potential in the treatment of hepatocellular carcinoma. Meanwhile, Cur enhances the PDT effect by inhibiting the expression of P-gp.

Experimental Section

Materials

Mice were obtained from Animal Research Center of China Medical University (Liaoning, China). ICG (99%) and Cur (98%) were obtained from Huafeng United Technology Co., Ltd (Beijing, China). Hydrogen chloride (HCl, 99%) and *n*-propyl alcohol (99%) were obtained from Beijing Chemical Corporation (Beijing, China). Thiourea ($[NH2]_2CS$, 99%) and sodium molybdate dehydrate (Na_2MoO_4 $2H_2O$, 99%) were purchased from Aladdin Bio-Chem Technology Co. (Shanghai, China). Scanning electron microscopy (SEM; S-4300, Hitachi) and Transmission electron microscopy (TEM; JEM-2100, JEOL) were used for morphologic characterization. UV-visible spectrophotometer (V-570, JASCO) was used to quantify the loading capacity and release rate of ICG and Cur. The temperature change in vitro and in vivo was monitored by an infrared thermal mapping apparatus (FLIR). Optical microscope (Olympus X71, Japan) was used to observe the morphology of the cells.

Synthesis of LMHSs

During this process, 0.6 g $Na_2MoO_4{\cdot}2H_2O$ and 0.8 g $(NH_2)_2$ CS were dissolved in 10 mL n-propyl alcohol and 50 mL deionized water. Two milliliters of HCl was used to adjust the acidity. Droplets obtained from the ultrasonic atomizer were taken through the furnace (600 °C) by a continuous flow of nitrogen. Subsequently, the products (LMHSs) were collected with ethanol. LMHSs were dried by freeze-drying after being kept in the fume hood for 24 hours.

Characterization

Transmission electron microscopy (TEM; JEM-2100, JEOL) and scanning electron microscopy (SEM; S-4300, Hitachi) were used for morphology observation.

Loading and Release of ICG and Cur

Ten milligrams of MoS_2, 10 mg ICG and 5 mg Cur were dissolved in 8 mL of mixture of tween80 and deionized

water in the dark place. Twenty minutes later, the solution was placed under vacuum condition until it was drained. The ICG&Cur@MoS_2 NPs were washed by the mixture of tween-80 and deionized water and centrifuged at 12,000 rpm for 6 min. The supernatant and washing solutions were collected and measured through a UV-visible spectrometer at 780 nmand 425 nm wavelength respectively to determine the drug-loading capacity. In order to determine the release rate at different pH values, the ICG&Cur@MoS_2 NPs were dispersed into mixture of tween80 and PBS with different pH values (5.5 and 7.4). The mixture of PBS solutions and NPs were placed at 37 °C under constant shaking. The supernatant of the ICG&Cur@MoS_2 solution was collected by centrifugation (12,000 rpm, 6 min) at different time points (0, 5, 10, 15, 30, 60, 120, 180, 240, 480, 720, and 1440 min), and then fresh PBS was added. The amount of ICG and Cur released at different time points was determined by a UV-visible spectrophotometer at 780 nm and 425 nm, respectively.

Photothermal Effect of ICG&Cur@MoS_2

NIR heating experiment was conducted to analyze the photothermal effect of ICG&Cur@MoS_2. Samples with different concentrations of ICG&Cur@MoS_2 (0.03, 0.06, 0.25, 1.00 mg/mL) were added into reaction vessels and irradiated by an 808 nm NIR laser at 2.0 W/cm^2 for 5 min to evaluate the photothermal effect of the ICG&Cur@MoS_2 NPs under NIR irradiation. FLIR was used to monitor changes of temperature. Pure water was used as the control group.

Cell Culture

HepG-2 cells (human hepatoma cells) were kindly given by Dr Qiong Wu (Laboratory of Controllable Preparation and Application of Nanomaterials, Chinese Academy of Sciences Key Laboratory of Cryogenics, Technical Institute of Physics and Chemistry, Chinese Academy of Sciences). The cells were incubated in DMEM (high-glucose) supplemented with 10% fetal bovine serum (FBS) and a 1% penicillin–streptomycin solution in a 5% CO_2 atmosphere.

Acute Toxicity in vivo

Up−down methods were performed to evaluate acute toxicity in vivo. Female mice were randomly allocated to four groups to evaluate the toxicity of the as-made ICG&Cur@MoS_2 NPs in vivo. Various doses of the ICG&Cur@MoS_2 (50, 100, and 200 mg/kg) were injected into the mice via tail vein. Mice treated with PBS were set as the control group. No loss of appetite or passive behavior was found even in the 200 mg/kg group. The mice were sacrificed after 20 days. Blood samples were used for biochemical and blood routine examination. Major organs (heart, liver, kidney, and lung) were separated and fixed in 10% formalin. Histological examination was conducted as the following procedures: paraffin embedding, sectioning, and staining with H&E. An optical microscope (Olympus X71) was used to observe the tissue section.

Therapeutic Experiment in vitro and in vivo

Methyl thiazolyl tetrazolium (MTT) assay was used to investigate the PTT-PDT effect in vitro. One hundred microliters of HepG-2 cells were cultured into 96-well plates (8×10^3 cells per well) for 12 h. Then, 100 μL of either ICG, MoS_2, ICG@MoS_2, or ICG&Cur@MoS_2, at the same concentration of ICG (0.5, 5, 25, 50 μg/mL), were added into each well. PBS was used to wash the cells and fresh culture medium was added after 2 h. Then, the cells were irradiated by an 808 nm NIR laser (1.2 W/cm^2) for 3 min. Twenty microliters of MTT solution was added into each well and the cells were incubated for another 3 h. Subsequently, 150 μL dimethyl sulfoxide (DMSO) was added to each well and the 96-well plates were shaken for a while. The absorbance was measured by a microplate reader at 492 nm.

Female ICR mice were purchased from Animal Research Center of China Medical University (Liaoning, China), and acclimated for 10 days. We injected H22 tumor cells (2×10^6) into the left hind of the mice. As the tumor grew to 200 mm^3, mice were randomly allocated into the following six groups: saline, ICG&Cur@MoS_2 + NIR, ICG&Cur + NIR, ICG@MoS_2 + NIR, MoS_2 + NIR, and NIR. The agents were injected into the mice through the tail vein. The injection dose of ICG&Cur@MoS_2, ICG@MoS_2, and MoS_2 was 40 mg/kg, whereas for the ICG&Cur + NIR group the dose was 15 mg/Kg. An 808 nm NIR laser (1.2 W/cm^2) was used to irradiate the tumors of the mice in the NIR groups, for 5 min, at 10 h post-injection. Both body weight and tumor size were measured and recorded carefully. The tumor size was calculated through the following formula: $V_{tumor} = ab^2/2$ (a and b represent length and width of the tumor, respectively). If the size of the tumor was larger than 20 mm in any one direction, the mice were sacrificed. All animal experiments were governed by the Regulations of Experimental

Animals of China Medical University (ethics approval number: 2019050, granted by Department of Laboratory Animal Science of China Medical University).

Cell Apoptosis Detection

Cells were fixed with 4% paraformaldehyde for 60 minutes at room temperature, and rinsed twice with PBS for 5 min each time. Three percent H_2O_2 was added and the cells were incubated for 10 min at room temperature. The cells were rinsed three times with distilled water, 2 min each time. One microliter of TdT and 1 μL DIG-dUTP were added to 18 μL labeling buffer to obtain reaction mixture. The reaction mixture was added to sample and the sample was incubated at 37 °C for 2 hours in a humidified atmosphere. The cells were rinsed with 0.01M TBS three times, 2 minutes each time. Then, the cells were incubated with blocking reagent for 30 min at room temperature. Biotin-conjugated anti-digoxin antibody was diluted with antibody dilution at the ratio of 1:100. The mixture was mixed well and 50 μL mixture was added to sample. The cells were rinsed with 0.01M TBS three times, 2 min each time. SABC was diluted in antibody dilution at the ratio of 1:100, the mixture was mixed well and 50 μL mixture was added to each sample. The cells were incubated at 37°C for 30 minutes in a humidified atmosphere. Then, 50 μL DAB mixture was added to each slide and the slides were incubated for 5–10 min at room temperature in the dark place. Then, the slides were counterstained for 5 minutes with hematoxylin.

Molecular Mechanism of the Inhibition of P-Gp by ICG&Cur@MoS_2

HepG-2 cells were cultured with ICG&Cur@MoS_2 in 24-well plates for 24 h. Then, the cells were lysed and collected after centrifugation. Bicinchoninic acid protein assay reagent was used to determine the total protein. The protein was resolved by sodium dodecyl sulfate-polyacrylamide gel electrophoresis. A polyvinylidene fluoride membrane was used to transfer the protein. The membranes were incubated in tris-buffered saline containing 0.1% TBST with 5% nonfat milk for 1 h. It was cultured with primary antibodies at 4 °C overnight. The blots were cultured with secondary antibody for 30 min after being washed two times and stained through an electrochemiluminescence detection kit. A chemiluminescent imaging system was used to photograph the signals. Real-time PCR was employed to further explore whether the inhibition occurs in the process of transcription or translation. TRIzol RNA isolation reagent was used to extract total RNA from HepG-2 cells. Forward primer and reversed primer of MDR1 is CCCATCATTGCAATAGCAGG and GTTCAAACTTCTG CTCCTCA. Forward primer and reversed primer of GAPDH are CTGGGCTACACTGAGCACC and AAGTGGTCGTT GAGGGCAATG, respectively. Reaction conditions of amplification curve are shown as follows: 95 °C, 5 min, 1 cycle; 95 °C, 5 s, 60 °C, 31 s, 40 cycles. Reaction conditions of dissociation curve are shown as follows: 95 °C, 15 s; 60 °C, 30 s; 95 °C, 15 s.

Statistical Analysis

The statistical analysis software used was SPSS Statistics. Statistical analyses were carried out by the Student's *t*-test. All experiments were repeated at least three times. The statistical significance was inferred at a value of $*p < 0.05$.

Results and Discussion

Synthesis and characterization of LMHSs

The microdroplets of the precursor solution were generated by an ultrasonic nebulization device. A flow of nitrogen was used to send the microdroplets into a furnace. Thiourea ($[NH_2]_2CS$) and sodium molybdate dehydrate (Na_2MoO_2 H_2O) were the precursors in our experiment. In Tan's study,[11] about 600 nm LMHSs were synthesized. The agents were delivered into tumor arterial of VX2 liver tumor in rabbits via transarterial administration (TA) under the guide of digital subtraction angiography (DSA). It is difficult for the LMHSs with a diameter of about 600 nm to penetrate the capillary into tumor tissue. As we know, nanomaterials should range from 100 to 400 nm to achieve the ideal EPR effect.[10] In this study, n-propyl alcohol was added to diminish the surface tension of the microdroplets, which made the NPs possess the ideal size for EPR effect. The LMHSs were obtained through reacting under the temperature of 600 °C. The SEM image indicates that the LMHSs possess spherical morphology (Figure 1B). According to the TEM image, the LMHSs possess hollow spherical and layered structures, which provide more space for antineoplastic drug (Figure 1A).

Loading and Release of ICG and Cur

It is suitable for the LHMSs to load antineoplastic agents.[10] ICG and Cur were loaded into the LMHSs by a vacuum negative pressure loading method. The ICG and Cur loading capacity was 33.7% and 36.9%, calculated through a standard curve, respectively. In Liu's work,[15] two-dimensional MoS_2 nanosheets were used to load anti-

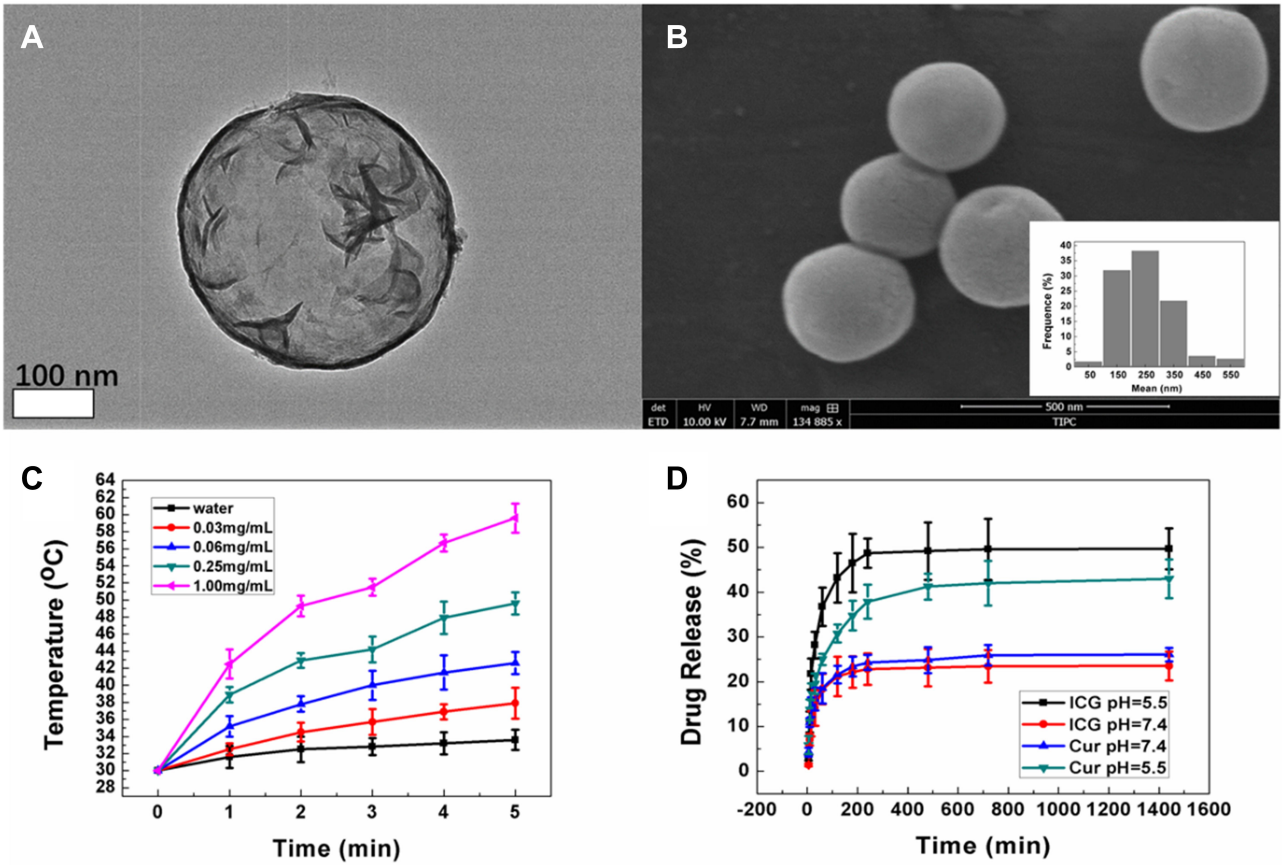

Figure 1 (**A**) The TEM image of LMHSs. (**B**) The SEM image and the average size of LMHSs. (**C**) In vitro temperature elevation curves of the ICG&Cur@MoS_2 NPs made at different concentrations under irradiation of an 808 nm NIR laser. (**D**) Drug release of ICG&Cur@MoS_2 NPs under different pH values.

cancer agents. However, the two-dimensional structure still limits drug loading. Compared with other molybdenum disulfide nanomaterials, the unique structures of the LMHSs provide more space for drug loading, which is the basis for further PDT-PTT. The controlled release effect of nanomaterials provides more opportunities for cancer treatment. Different from normal tissues, cancer tissues rely mainly on glycolysis to provide energy (warburg effect).[16,17] Tumor tissue is acidic due to accumulation of lactic acid by glycolysis, which provides a basis for controlled release.[18] In our previous study, controlled release nanoplatforms-doxorubicin-loaded layered MoS_2 hollow spheres-were successfully constructed. It depended on the difference of pH between blood and tumor to achieve controlled release.[10] To explore the release behavior in vitro, the ICG&Cur@MoS_2 NPs were dispersed into PBS solution with different pH values (5.5 and 7.4) at the temperature of 37 °C. The released ICG from the ICG&Cur@MoS_2 NPs was 45.2% and 20.1% at 12 h when the pH value was 5.5 and 7.4. Similarly, the releasing rate of Cur reached 41.3% at 12 h when the pH value was 5.5, and 25.2% at pH 7.4 (Figure 1D). These findings indicate that ICG and Cur can be more easily released in tumor issue, which may be attributed to the weak acidity of cancer tissue. In Bishara's research,[19] ICG distribution into the fetus was enhanced when rifampin was used. Besides, plenty of commonly used P-gp inhibitors, such as rifampin and valspodar, may cause serious side effects to patients.[7,9,12] Patients with hepatocellular carcinoma are often accompanied by hepatic insufficiency, so rifampin is prohibitive in those patients.[12] However, P-gp is the obstacle in HCC therapy. In our study, as a natural plant ingredient, curcumin not only shows high biological safety but also can be released more easily in tumor tissue.[13,14]

Photothermal Properties of ICG&Cur@MoS_2 in vitro

Photothermal conversion is the basis of PTT. MoS_2 has been widely studied as a kind of nanomaterials with high photothermal conversion. In Liu's work,[15] MoS_2 nanosheets, a kind of two-dimensional nanomaterials, have been applied to cancer treatment. In our work, LHMSs

possess a three-dimensional structure, making it more suitable for loading anti-cancer agents. There was no obvious change of temperature in water after 5 min at 2.0 W/cm^2 and 808 nm NIR irradiation, while the temperature of the 0.06 mg/mL group was increased to 43.6 °C. In the 1.00 mg/mL group, the highest temperature was 60.7 °C after irradiation for 5 min, which indicated that ICG&Cur@MoS_2 NPs exhibited an excellent photothermal effect (Figure 1C).

Acute Toxicity Evaluation

To test the acute toxicity of ICG&Cur@MoS_2 in vivo, different doses (50, 100, and 200 mg/Kg) of ICG&Cur@MoS_2 were injected into the mice via tail vein. The full blood count, including platelet (PLT), hemoglobin (HGB), mean corpuscular volume (MCV), mean capacity hemoglobin (MCH), mean corpuscular hemoglobin concentration (MCHC), white blood cells (WBC) and red blood cells (RBC), and biochemical indices, including alanine aminotransferase (ALT), aspartate aminotransferase (AST), creatinine (CREA), and urea (UREA) were evaluated, respectively. Meanwhile, the body weight of mice in each group has been carefully recorded. Even in the 200 mg/kg group, no loss of appetite or passive behavior was observed. As expected, no significant differences of body weight were found in each group when compared with the control group (Figure 2A). In addition, major organs (heart, liver, spleen, kidney, and lung) from mice of each group were collected for pathological study. No severe pathological changes such as inflammation or fibrosis were observed in H&E-stained sections (Figure 2B). These results indicated that the toxicity of the ICG&Cur@MoS_2 NPs was relatively low. In Tan's study,[11] LMHSs have negligible toxic effects to normal tissues and blood through systematic acute toxicity study. In addition, in Li's study, doxorubicin-loaded layered MoS_2 (DOX@MoS_2) hollow spheres as a synergistic treatment platform shows great clinical potential. Therefore, MoS_2 nanomaterials have very high biocompatibility. The high biocompatibility of ICG&Cur@MoS_2 may be reasonably attributed to the following three facts: first, in many previous studies, LMHSs have been proved to be highly biocompatible to organisms; second, ICG has been used for many years in clinic, with no serious adverse actions;[20,21] third, as a kind of polyphenol compounds extracted from curcuma, Cur is widely used as food additives for a long time. In summary, the ICG&Cur@MoS_2 NPs exhibit remarkable biocompatibility.

PTT-PDT in vitro and in vivo

Because of the heterogeneity of tumors, it is difficult to treat tumors with a single treatment. More and more research has been focused on synergistic therapy in cancer. In Li's study,[5] as a synchronous photodynamic–photothermal therapy platform, gold nanospheres-stabilized indocyanine green inhibits tumor growth and metastasis. Encouraged by the above findings, we further tested the PTT-PDT effect of ICG&Cur@MoS_2. MTT assay was used to investigate the

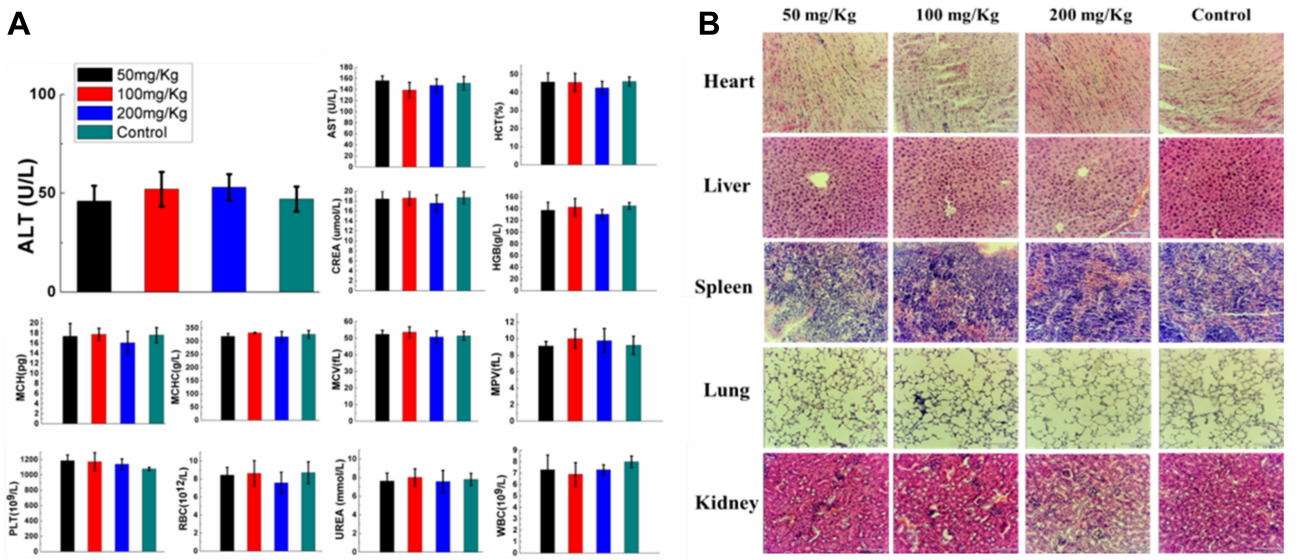

Figure 2 (**A**) In vivo acute toxicity evaluation of the ICG&Cur@MoS_2 NPs made at various concentrations (50, 100, 200 mg kg^{-1}, with PBS-treated group as the control). Blood biochemistry including ALT, AST, CREA, and UREA and blood routine including MCHC, PLT, MCH, MCV, HCT, HGB, RBC, WBC, and MPV of each group. (**B**) Evaluation of acute toxicity of the ICG&Cur@MoS_2 NPs made at various concentrations (50, 100, 200 mg kg^{-1}, with PBS-treated group as the control). Images of H&E staining of major organs (heart, liver, kidney, and lung) from mice of each group. The scale bar is 120 μm.

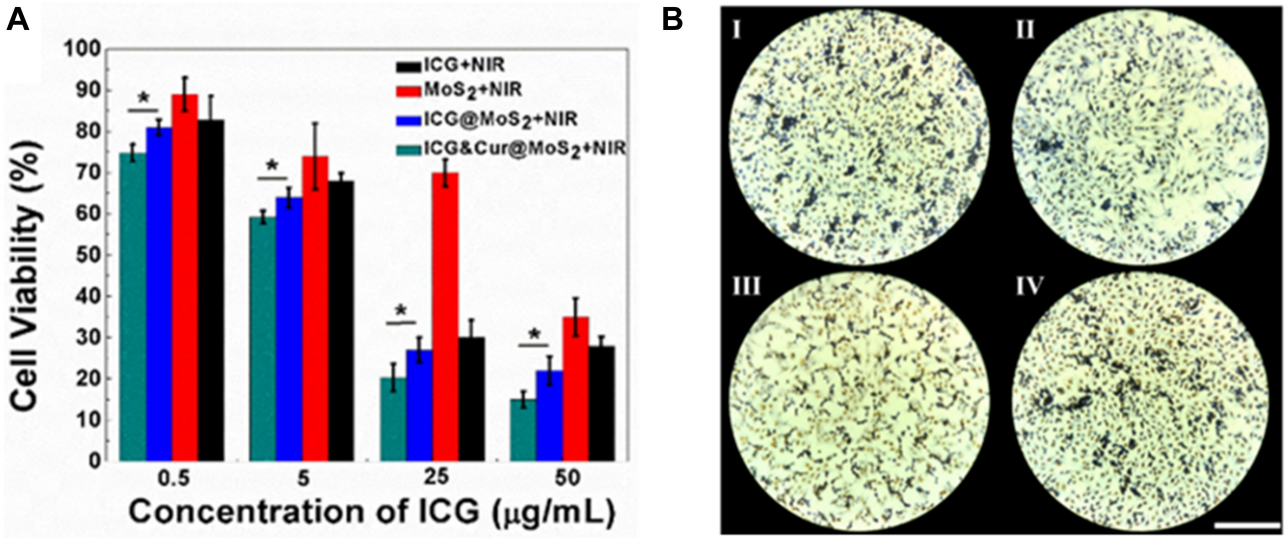

Figure 3 (**A**) Cell viabilities of HepG-2 cells under different treatments indicated. In this section, cells were incubated with ICG, MoS_2, ICG@MoS_2, and ICG&Cur@MoS_2 at the same ICG concentration (0.5, 5, 25, 50 μg/mL) for 2 h (the concentration of MoS_2 in the MoS_2 + NIR group was consistent with corresponding concentration in ICG@MoS_2 + NIR and ICG&Cur@MoS_2 + NIR group), and then irradiated by an 808 nm laser. Then the MTT assay was used to detect the cell viability. (**B**) Apoptosis detection of cells under different treatments. I: ICG + NIR, II: MoS_2 + NIR, III: ICG@MoS_2+ NIR, IV: ICG&Cur@MoS_2 + NIR. The ICG concentration is 50 μg/mL (the concentration of MoS_2 in the MoS_2 + NIR group was consistent with corresponding concentration in ICG@MoS_2 + NIR and ICG&Cur@MoS_2 + NIR group). Yellow cells are the apoptotic cells. The bar is 180 μm. *p < 0.05.

PTT-PDT effect in vitro (Figure 3A). After Cur was integrated into ICG@MoS_2, the inhibition of HepG-2 cells was obviously enhanced. Cell viability in the ICG&Cur@MoS_2 + NIR group was significantly lower than that in ICG@MoS_2 + NIR group (75.3% vs 81.2%, 59.0% vs 64.4%, 20.3% vs 27.5%, and 15.4% vs 22.3%) at the concentration of ICG at 0.5, 5, 25, 50 μg/mL (P<0.05 at each concentration). The results may be attributed to the synergistic effect of PTT - PDT and inhibition of P-gp. TUNEL assay was used to further explore the cell death in this study. As we know, apoptosis is one of the most important type of cell death.[22–24] Endonucleolysis is considered as the key biochemical event of apoptosis, which will result in double-stranded, low-molecular-weight DNA fragments as well as single-strand breaks in high-molecular-weight DNA. As a result, TUNEL assay can be used to identify the apoptosis

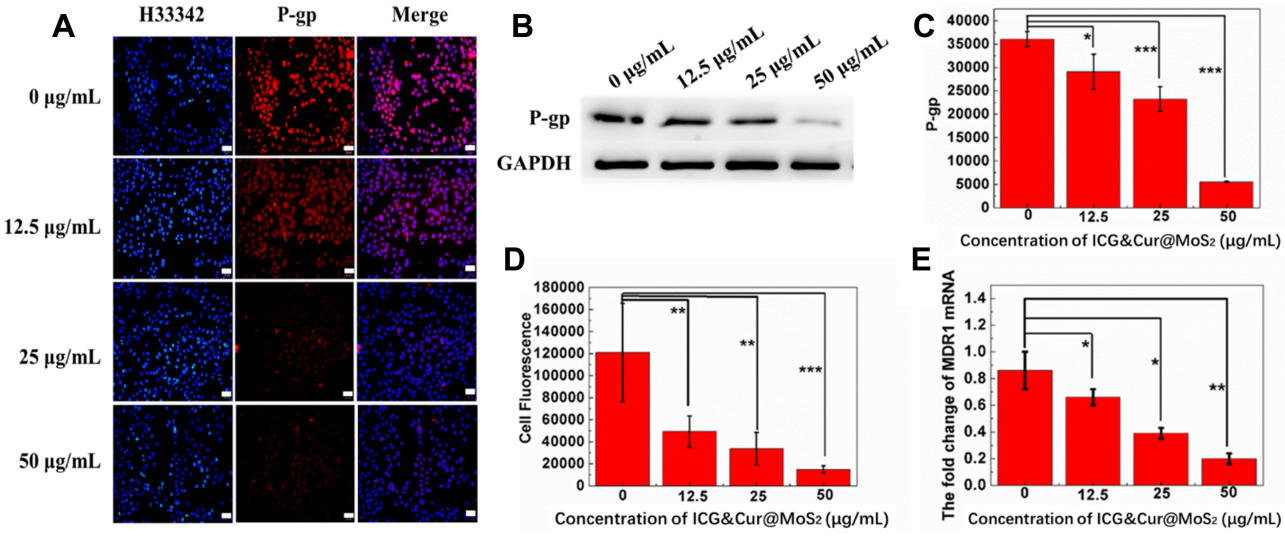

Figure 4 (**A**) Immunofluorescence of HepG-2 cells treated with ICG&Cur@MoS_2 at different concentrations (0, 12.5, 25, and 50 μg/mL). The bar is 50 μm. (**B**) The expression of P-gp under different concentrations (0, 12.5, 25, and 50 μg/mL) by Western blot. (**C**) Semi-quantitative analysis of (**B**). (**D**) Semi-quantitative analysis of (**A**). (**E**) The change of MDR1 mRNA under different concentrations (0, 12.5, 25, and 50 μg/mL). *p < 0.05, **p < 0.01, and ***p < 0.001.

cells. As shown in Figure 3B, significant apoptosis cells were found in ICG@MoS_2 + NIR group, indicating that apoptosis was involved in the cell death induced by heat and ROS. Many studies have shown that intracellular ICG concentration is significantly increased through inhibiting P-gp. In Guo's work,[25] near-infrared laser-triggered nitric oxide nanogenerators were used for MDR cancer therapy. In their study, nitric oxide (NO) was used to inhibit the expression of P-gp and it showed positive results. As we know, as an important signal molecule, NO involves in various physiological activities, especially in cardiovascular system.[26,27] The accumulation of NO may cause side effects in cardiovascular system. Therefore, it may not be a proper P-gp inhibitor for clinic. It is critical to find a safe and effective P-gp inhibitor. In this work, as a kind of polyphenol compounds extracted from curcuma, Cur is widely used as food additives for a long time.[13,14] In Rejinold's research,[28] Cur was used as a novel nanocarrier system for doxorubicin delivery to inhibit MDR. Therefore, ICG&Cur@MoS_2 may have greater potential for clinical usage. In this study, Western blot, Q-PCR, and immunofluorescence assay were used to further explore the mechanism of the inhibition of P-gp by ICG&Cur@MoS_2. Western blot was used to evaluate the expression of P-gp (Figure 4B and C). The results of Western blotting were semi −quantified by an image analysis software (Image J). Compared with the control group, the P-gp of HepG-2 cells treated with ICG&Cur@MoS_2 was significantly inhibited ($p<0.05$, $p<0.001$ and $p<0.001$). The results are consistent with immunofluorescence (Figure 4A and D). Fluorescence of cells treated with ICG&Cur@MoS_2 was significantly weaker than that in the control group ($p<0.01$, $p<0.01$ and $p<0.001$). As we know, the expression of protein requires

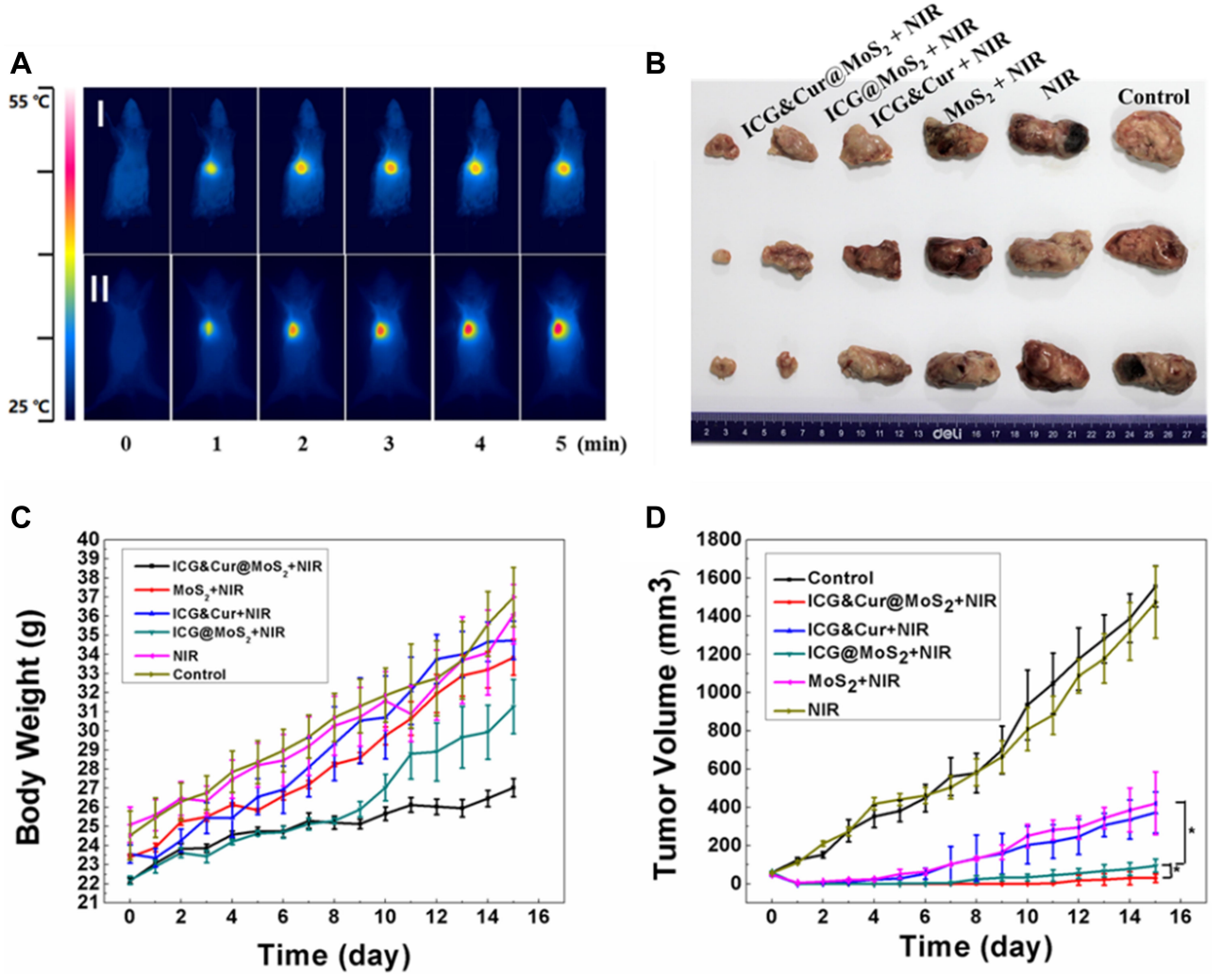

Figure 5 (**A**) Infrared thermography in vivo (I: control group. II: ICG&Cur@MoS_2 + NIR group). (**B**) Ex vivo photographs of H22 tumors. (**C**) Body weight curve of each group. (**D**) Tumor growth curve of each group. *$p < 0.05$.

three basic steps: DNA replication, transcription and translation. Intervention at any step may affect the expression of protein. P-gp is encoded by MDR1.[9] Real-time PCR was employed to further explore whether the inhibition occurs in the process of transcription or translation. As shown in Figure 4E, mRNA was significantly decreased in the ICG&Cur@MoS_2 group, indicating that ICG&Cur@MoS_2 inhibited the transcription of MDR1. The tumor microenvironment is extremely complex with a series of characteristics like acidosis, interstitial hypertension, inflammatory cell infiltration and so on.[29–32] As a result, we further explored the PTT-PDT effect in vivo (Figure 5A, B and D). Interestingly, the body weight in control group is higher than that of other groups, which is attributed to uncontrolled growth of tumors (Figure 5C). The tumors in the ICG@MoS_2 + NIR group are significantly smaller than those in the MoS_2 + NIR group (95.0 vs 420.9 mm^3, $p<0.05$). As previously described, the abundant blood supply of liver cancer will adversely affect thermal ablation. However, photodynamic therapy may benefit from the oxygen-enriched microenvironment. Combining PTT and PDT will compensate for the drawbacks of single PTT or PDT in cancer treatment. As a result, PTT and PDT synergetic therapy exhibits satisfactory effect. However, compared with the ICG@MoS_2 + NIR group, the tumors in the ICG&Cur@MoS_2 + NIR group had been more effectively controlled (95.0 vs 29.6 mm^3 $p<0.05$). The results may be attributed to the inhibition of P-gp, which will enhance the PDT effect. P-gp, which is encoded by MDR1, is one of the main barriers in tumor therapy, inducing multidrug resistance and attenuating PDT.[33–35] In recent years, many scientists have devoted to the study of P-glycoprotein inhibition, while most of the P-gp inhibitors have serious adverse reactions. In our study, as a safe and effective P-gp inhibitor, Cur was loaded into the LMHSs to inhibit the P-gp. The results have showed that ICG&Cur@MoS_2 can significantly enhance the therapy effect.

Conclusion

In conclusion, we have successfully synthesized ICG&Cur@MoS_2 nanoparticles which can not only achieve PTT-PDT but also inhibit P-gp effectively. Cur is much safer than traditional P-gp inhibitors. The unique structure of LMHSs provides more space for anti-tumor agents. Our findings indicate that the PTT-PDT exhibits great potential in the treatment of hepatocellular carcinoma. Meanwhile, ICG&Cur@MoS_2 can effectively inhibit the expression of P-gp, which will enhance the PDT effect.

Acknowledgments

The authors acknowledge the financial support from the National Natural Science Foundation of China (81771944, 82072037, 8201101264), National Hi-Technology Research and Development Program (863 Program) (2012AA022701), Liaoning Innovative Talents Supporting Program, and Shenyang Innovative Talents Supporting Program (No. RC170048).

Disclosure

The authors report no conflicts of interest for this work.

References

1. Jin Y, Yang X, Tian J. Targeted polypyrrole nanoparticles for the identification and treatment of hepatocellular carcinoma. *Nanoscale*. 2018;10:9594. doi:10.1039/C8NR02036A
2. Han Y, An Y, Jia G, et al. Theranostic micelles based on upconversion nanoparticles for dual-modality imaging and photodynamic therapy in hepatocellular carcinoma. *Nanoscale*. 2018;10:6511. doi:10.1039/C7NR09717D
3. Li W, Yang J, Luo L, et al. Targeting photodynamic and photothermal therapy to the endoplasmic reticulum enhances immunogenic cancer cell death. *Nat Commun*. 2019;10:3349. doi:10.1038/s41467-019-11269-8
4. Pinto A, Pocard M. Photodynamic therapy and photothermal therapy for the treatment of peritoneal metastasis: a systematic review. *Pleura Peritoneum*. 2018;3:20180124. doi:10.1515/pp-2018-0124
5. Li W, Zhang H, Guo X, et al. Gold nanospheres-stabilized indocyanine green as a synchronous photodynamic-photothermal therapy platform that inhibits tumor growth and metastasis. *ACS Appl Mater Interfaces*. 2017;9:3354. doi:10.1021/acsami.6b13351
6. Song W, Li Y, Wang Y, et al. Indocyanine green-loaded gold nanoflowers@two layers of silica nanocomposites for photothermal and photodynamic therapy of oral carcinoma. *J Biomed Nanotechnol*. 2017;13:1115. doi:10.1166/jbn.2017.2409
7. Robinson K, Tiriveedhi V. Perplexing role of P-glycoprotein in tumor microenvironment. *Front Oncol*. 2020;10:265. doi:10.3389/fonc.2020.00265
8. Li S, Gao M, Li Z, et al. p53 and P-glycoprotein influence chemoresistance in hepatocellular carcinoma. *Front Biosci (Elite Ed)*. 2018;10:461.
9. Tanaka K, Kiguchi K, Mikami M, et al. Involvement of the MDR1 gene and glycolipids in anticancer drug-resistance of human ovarian carcinoma-derived cells. *Hum Cell*. 2019;32:447. doi:10.1007/s13577-019-00261-5
10. Li S, Tan LF, Xu WH. Doxorubicin-loaded layered MoS2 hollow spheres and its photothermo-chemotherapy on hepatocellular carcinoma. *J Biomed Nanotechnol*. 2017;13:1557. doi:10.1166/jbn.2017.2461
11. Tan L, Wang S, Xu K, et al. Layered MoS2 hollow spheres for highly-efficient photothermal therapy of rabbit liver orthotopic transplantation tumors. *Small*. 2016;12:2046. doi:10.1002/smll.201600191
12. Elmeliegy M, Vourvahis M, Guo C, et al. Effect of P-glycoprotein (P-gp) inducers on exposure of P-gp substrates: review of clinical drug-drug interaction studies. *Clin Pharmacokinet*. 2020;59(6):699–714. doi:10.1007/s40262-020-00867-1
13. Lestari ML, Indrayanto G. Curcumin. *Profiles Drug Subst Excip Relat Methodol*. 2014;39:113.
14. Priyadarsini KI. The chemistry of curcumin: from extraction to therapeutic agent. *Molecules*. 2014;19:20091. doi:10.3390/molecules191220091

15. Liu T, Wang C, Gu X, et al. Drug delivery with PEGylated MoS2 nano-sheets for combined photothermal and chemotherapy of cancer. *Adv Mater*. 2014;26:3433. doi:10.1002/adma.201305256
16. Liberti MV, Locasale JW. The warburg effect: how does it benefit cancer cells. *Trends Biochem Sci*. 2016;41:211. doi:10.1016/j.tibs.2015.12.001
17. Kimmelman AC, White E. Autophagy and tumor metabolism. *Cell Metab*. 2017;25:1037. doi:10.1016/j.cmet.2017.04.004
18. Vaupel P, Schmidberger H, Mayer A. The warburg effect: essential part of metabolic reprogramming and central contributor to cancer progression. *Int J Radiat Biol*. 2019;95:912. doi:10.1080/09553002.2019.1589653
19. Ameer B, Michal M, Emma P, et al. Near infrared imaging of indocyanine green distribution in pregnant mice and effects of concomitant medications. *Mol Pharm*. 2015;12:3351. doi:10.1021/acs.molpharmaceut.5b00374
20. Kaplan-Marans E, Fulla J, Tomer N, et al. Indocyanine green (ICG) in urologic surgery. *Urology*. 2019;132:10. doi:10.1016/j.urology.2019.05.008
21. Esposito C, Del Conte F, Cerulo M, et al. Clinical application and technical standardization of indocyanine green (ICG) fluorescence imaging in pediatric minimally invasive surgery. *Pediatr Surg Int*. 2019;35:1043. doi:10.1007/s00383-019-04519-9
22. Elmore S. Apoptosis: a review of programmed cell death. *Toxicol Pathol*. 2007;35:495. doi:10.1080/01926230701320337
23. D'Arcy MS. Cell death: a review of the major forms of apoptosis, necrosis and autophagy. *Cell Biol Int*. 2019;43:582. doi:10.1002/cbin.11137
24. Qiao L, Wong BC. Targeting apoptosis as an approach for gastrointestinal cancer therapy. *Drug Resist Updat*. 2009;12:55. doi:10.1016/j.drup.2009.02.002
25. Guo RR, Tian Y, Wang YJ, et al. Near-infrared laser-triggered nitric oxide nanogenerators for the reversal of multidrug resistance in cancer. *Adv Funct Mater*. 2017;27:1606398. doi:10.1002/adfm.201606398
26. Farah C, Michel LYM, Balligand JL. Nitric oxide signalling in cardiovascular health and disease. *Nat Rev Cardiol*. 2018;15:292.
27. Moncada S, Higgs EA. The discovery of nitric oxide and its role in vascular biology. *Br J Pharmacol*. 2006;147(Suppl 1):S193. doi:10.1038/sj.bjp.0706458
28. Rejinold NS, Yoo J, Jon S, et al. Curcumin as a novel nanocarrier system for doxorubicin delivery to MDR cancer cells: in vitro and in vivo evaluation. *ACS Appl Mater Interfaces*. 2018;10:28458. doi:10.1021/acsami.8b10426
29. Wu T, Dai Y. Tumor microenvironment and therapeutic response. *Cancer Lett*. 2017;387:61. doi:10.1016/j.canlet.2016.01.043
30. Hanahan D, Coussens LM. Accessories to the crime: functions of cells recruited to the tumor microenvironment. *Cancer Cell*. 2012;21:309. doi:10.1016/j.ccr.2012.02.022
31. Cheng W, Liang C, Wang X, et al. A drug-self-gated and tumor microenvironment-responsive mesoporous silica vehicle: "four-in-one" versatile nanomedicine for targeted multidrug-resistant cancer therapy. *Nanoscale*. 2017;9:17063. doi:10.1039/C7NR05450E
32. An M, Yu C, Xi J. Induction of necrotic cell death and activation of STING in the tumor microenvironment via cationic silica nanoparticles leading to enhanced antitumor immunity. *Nanoscale*. 2018;10:9311. doi:10.1039/C8NR01376D
33. Szakács G, Paterson JK, Ludwig JA, et al. Targeting multidrug resistance in cancer. *Nat Rev Drug Discov*. 2006;5:219.
34. Li W, Zhang H, Assaraf YG, et al. Overcoming ABC transporter-mediated multidrug resistance: molecular mechanisms and novel therapeutic drug strategies. *Drug Resist Updat*. 2016;27:14. doi:10.1016/j.drup.2016.05.001
35. Zhou L, Wang H, Li Y. Stimuli-responsive nanomedicines for overcoming cancer multidrug resistance. *Theranostics*. 2018;8:1059. doi:10.7150/thno.22679